Engineering of a synthetic electron conduit in living cells

Heather M. Jensen[a,b], Aaron E. Albers[c], Konstantin R. Malley[c,1], Yuri Y. Londer[d], Bruce E. Cohen[c], Brett A. Helms[c], Peter Weigele[d], Jay T. Groves[a,b,c,e], and Caroline M. Ajo-Franklin[b,c,2]

[a]Departments of Chemistry and [e]Howard Hughes Medical Institute, University of California, Berkeley, CA 94720; [b]Physical Biosciences and [c]Materials Sciences Divisions, Lawrence Berkeley National Laboratory, University of California, Berkeley, CA 94720; and [d]New England Biolabs, Ipswich, MA 01938

Edited by Charles R. Cantor, Sequenom, Inc., San Diego, CA, and approved September 8, 2010 (received for review July 2, 2010)

Engineering efficient, directional electronic communication between living and nonliving systems has the potential to combine the unique characteristics of both materials for advanced biotechnological applications. However, the cell membrane is designed by nature to be an insulator, restricting the flow of charged species; therefore, introducing a biocompatible pathway for transferring electrons across the membrane without disrupting the cell is a significant challenge. Here we describe a genetic strategy to move intracellular electrons to an inorganic extracellular acceptor along a molecularly defined route. To do so, we reconstitute a portion of the extracellular electron transfer chain of *Shewanella oneidensis* MR-1 into the model microbe *Escherichia coli*. This engineered *E. coli* can reduce metal ions and solid metal oxides ∼8× and ∼4× faster than its parental strain. We also find that metal oxide reduction is more efficient when the extracellular electron acceptor has nanoscale dimensions. This work demonstrates that a genetic cassette can create a conduit for electronic communication from living cells to inorganic materials, and it highlights the importance of matching the size scale of the protein donors to inorganic acceptors.

cytochrome c | nanobioelectronics | synthetic biology | iron reduction | living-nonliving interfaces

Both organisms and human-made technological devices use the flow of charge as information and energy. Creating an interface that permits electrical communication between living and nonliving systems would enable previously undescribed opportunities in fields such as biosensing, bioenergy, and cellular engineering. Sophisticated pipette- and electrode array-based techniques permit transfer of ions from electrogenic and nonelectrogenic cells to electrodes (1, 2). Although most technological devices are electronic (i.e., rely on electron flow), a limited set of techniques are available to permit transfer of electrons from a variety of cell types to electrodes. Lipid-soluble mediators or combinations of mediators can be used to transport electrons from intracellular redox enzymes to extracellular electrodes in bacterial (3, 4), fungal (5), and mammalian cells (6), but such mediators rely on diffusion to interact with multiple cellular substrates, thus obscuring a molecular-level understanding of the electron path. Alternatively, in the absence of exogenous mediators, a limited set of bacterial species are able to directly transfer electrons to electrodes (7–9). However, a general strategy to create cell-electrode connections with a well-defined electron transfer path that is broadly applicable to many cell types has remained elusive.

To make electrical connections to cells, most approaches rely on introduction of noncellular redox species (10, 11) or physical means to abrogate the inherently electrically insulating character of cellular membranes (12). Here we explore a radically different, biologically focused approach: to use synthetic biology to introduce an electron transfer pathway that routes electrons along a well-defined path from the cell interior to an extracellular inorganic material. This approach specifically takes advantage of a natural electron pathway that has evolved to utilize a variety of solid metals and metal oxides as terminal electron acceptors. Because such an extracellular electron transfer pathway is absent in most cell types, we have the ability to create a well-defined electron path with precise and flexible control over the combination and localization of the electron-carrying proteins. This approach is now tractable in part because the advent of genome sequencing has greatly added to the molecular-level understanding of diverse organisms (13, 14). Also key to this approach, the growing field of synthetic biology offers more sophisticated tools available to create and modify genetic systems (15–20). Now armed with greater control over translation and transcription of synthetic genes and pathways (21, 22), it is possible to engineer the living cell as a material for advanced biological systems and applications.

Naturally occurring dissimilatory metal-reducing bacteria, such as those from the genera *Shewanella* and *Geobacter*, have evolved mechanisms for direct charge transfer to inorganic minerals, enabling them to use solid metal oxides as terminal electron acceptors during anaerobic respiration (23–25). The electron transfer pathway of *Shewanella oneidensis* MR-1, one of the best understood pathways, is comprised of c-type cytochromes that shuttle electrons from cytoplasmic and inner membrane oxidizing enzymes toward the outside of the cell during anaerobic respiration. Extensive genetic and biochemical data suggest that the major components of the *S. oneidensis* MR-1 electron transfer pathway are an inner membrane tetraheme cytochrome CymA, a periplasmic decaheme cytochrome MtrA, outer membrane decaheme cytochromes OmcA and MtrC, and an outer membrane β-barrel protein MtrB (Fig. 1*A*) (26–30). This pathway is proposed to move electrons from the intracellular quinol pool to extracellular metal oxides, such as Fe_2O_3 (s), via a series of intermolecular electron transfer events from quinol to CymA, from CymA to MtrA, and from MtrA to either MtrC and/or OmcA.

In this work, we set out to determine whether we could convert a bacterial strain that is incapable of reducing solid metal oxides to one that can by installing a synthetic electron conduit that bridges the cytosol to the extracellular space. To do so, we expressed the MtrC, MtrA, and MtrB proteins from *S. oneidensis* MR-1 in *Escherichia coli*. In this heterologous system, we find that the mature proteins are functionally expressed, and MtrC and MtrA are redox active. We present evidence that MtrA interacts with at least one native *E. coli* redox protein and that it has a direct role in accelerating the rate of soluble Fe(III) reduction. Most importantly, we show that expression of *mtrCAB* can "wire

Author contributions: H.M.J., Y.Y.L., P.W., J.T.G., and C.M.A.-F. designed research; H.M.J. and K.R.M. performed research; A.E.A., B.E.C., and B.A.H. contributed new reagents/analytic tools; H.M.J., Y.Y.L., P.W., and C.M.A.-F. analyzed data; and H.M.J. and C.M.A.-F. wrote the paper.

The authors declare no conflict of interest.

This article is a PNAS Direct Submission.

[2]To whom correspondence should be addressed. E-mail: cajo-franklin@lbl.gov.

[1]Present address: Saint Louis University School of Medicine, St. Louis, MO 63104.

This article contains supporting information online at www.pnas.org/lookup/suppl/doi:10.1073/pnas.1009645107/-/DCSupplemental.

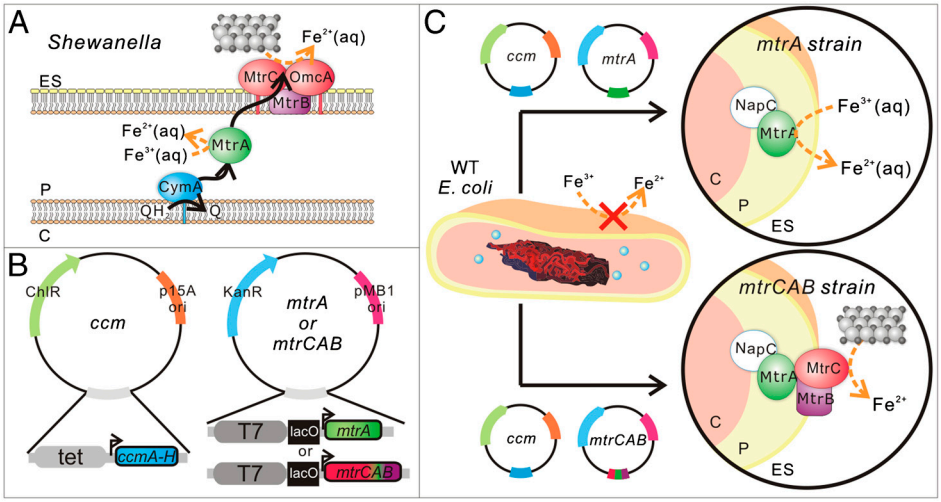

Fig. 1. (*A*) Schematic of proposed extracellular electron transfer pathway in *Shewanella oneidensis* MR-1 where ES denotes the extracellular space, P denotes the periplasm, and C denotes the cytoplasm. The silver and black spheres represent extracellular iron oxide. (*B*) Schematic of plasmids used to create the *ccm*, *mtrA*, and *mtrCAB* strains in *E. coli*. (*C*) Schematic of the engineered *mtrA* and *mtrCAB* strains for soluble and extracellular metal reduction.

up" *E. coli* to inorganic solids; i.e., it confers the ability to reduce solid α-Fe_2O_3 and the rate of electron flow is increased when the solid has nanometer dimensions.

Results

Design of the Synthetic Electron Conduit Using *S. oneidensis* MR-1 *mtrCAB*. Because it is a genetically tractable, gram-negative bacterium with readily available tools for heterologous expression of cytochromes c, *E. coli* was chosen as a test bed to determine whether we could genetically introduce a molecularly defined electron conduit modeled on the extracellular electron transfer pathway of *S. oneidensis* MR-1. The physical arrangement of *S. oneidensis* MR-1 cytochromes (Fig. 1*A*) suggests that an inner membrane, a periplasmic, and an outer membrane cytochrome are required to achieve extracellular electron transfer in *E. coli*. In support of this hypothesis, although CymA (31, 32), MtrA (32, 33), OmcA (34), and the combination of MtrA and CymA (32) have been expressed in *E. coli*, none of these systems has been shown sufficient to reduce solid Fe(III) oxides to Fe(II). Additionally, published reports suggest that the outer membrane 28 strand β-barrel protein MtrB is required for correct folding and localization of MtrC and OmcA (35) and may be involved in interactions between MtrC and MtrA (36). Yet, because extensive posttranslational processing is required to correctly incorporate the multiple hemes, fold, and localize each of these cytochromes c, heterologous expression of even a single multiheme cytochrome c is a significant technical challenge. To our knowledge, multiple decaheme cytochromes have not been simultaneously expressed in *E. coli*, so we sought to select a minimal number of proteins to heterologously express. The work of both Gescher and Pitts suggest that the native *E. coli* inner membrane tetraheme cytochrome NapC, which is 52% sequence similar to CymA, can reduce heterologously expressed MtrA (31, 33). Therefore, we selected the *mtrCAB* genes as a potentially minimal set required to create a synthetic electron conduit that would allow *E. coli* to reduce insoluble metal oxides. To allow us to dissect the electron transfer paths of this heterologous pathway and to separately investigate the role of MtrA and MtrC in Fe(III) reduction, we also chose to express MtrA by itself (Fig. 1 *B* and *C*).

Functional Expression of *mtrC*, *mtrA*, and *mtrB* in *E. coli*. We created two plasmids containing *mtrA* and *mtrCAB* under the control of a *T7 lac* promoter (Fig. 1*B*) (37, 38). Because the *E. coli* cytochrome c maturation (*ccmABCDEFGH*) genes are required for heme insertion but are not transcribed under aerobic conditions (39), the *mtrA* and *mtrCAB* plasmids were cotransformed with pEC86 (Fig. 1*C*), a cytochrome c maturation (*ccm*) plasmid containing *ccmA-H* under the constitutive *tet* promoter (Fig. 1*B*) (40) into BL21(DE3) cells. BL21(DE3) cells (WT strain) and cells carrying only the *ccm* plasmid (*ccm* strain) were pale yellow in color; conversely, cells containing both the *ccm* and *mtrA* (*mtrA* strain) or *mtrCAB* (*mtrCAB* strain) plasmids were red (S4), indicating that the cytochromes were expressed. Addition of isopropyl β-D-1-thiogalactopyranoside (IPTG), which derepresses the *T7 lac* promoter, would be expected to increase expression of MtrA and MtrCAB in the *mtrA* and *mtrCAB* strains, respectively. However, even low concentrations of IPTG (10 μM) resulted in cell pellets with a less intense red color as compared to the same strain uninduced, suggesting more protein was expressed under noninducing conditions; therefore, we performed all subsequent growth in the absence of IPTG.

In *S. oneidensis* MR-1, the periplasmic and outer membrane localization of MtrA and MtrC are believed to be crucial for extracellular electron transfer (26). To probe the localization of heterologously expressed MtrA and MtrC, aerobically grown WT, *ccm*, *mtrA*, and *mtrCAB* strains were fractionated into periplasmic and membrane fractions. These fractions were analyzed by SDS-PAGE followed by 3,3′,5,5′-tetramethylbenzidine (TMBZ) staining, which stains proteins with covalently bound heme (41). The periplasmic and membrane fractions of WT and *ccm* strains had no visible bands in the TMBZ stain, suggesting that no or little native c-type cytochrome is present (Fig. 2 *A* and *B*). The periplasmic fractions of both *mtrA* and *mtrCAB* strains had a band at 32 kD, the expected molecular mass of MtrA, indicating that MtrA is correctly targeted to the periplasm (Fig. 2*A*). MtrA is present to a lesser degree in the membrane fractions of both strains, whereas a band at the expected molecular mass of MtrC, 71 kD, is present only in the membrane fraction of the *mtrCAB* strain (Fig. 2*B*). Finally, only the membrane fraction of the *mtrCAB* strain produced a band at the expected molecular mass of MtrB, 77 kD, in an immunoblot with an MtrB-specific antibody (Fig. 2*C*). This pattern of localization for MtrA, MtrB, and MtrC in *E. coli* is identical to that reported for *S. oneidensis* MR-1, indicating that heterologous expression preserved these proteins' native localizations (27, 33, 42).

The MtrCAB proteins must also be redox active for functional electron transport. We probed the redox activity of heterologously expressed MtrA and MtrC using UV-Vis absorption spectroscopy. The visible spectra of the periplasm and membrane fractions of *mtrA* and *mtrCAB* strains were obtained under oxidizing (air) and reducing conditions (sodium dithionite). The most prominent features of oxidized c-type cytochromes are the Soret band at 410 nm and a broad second peak at 530 nm. After chemical reduction with sodium dithionite, the Soret band shifts to 420 nm and the β- and α-bands are seen at 525 nm and

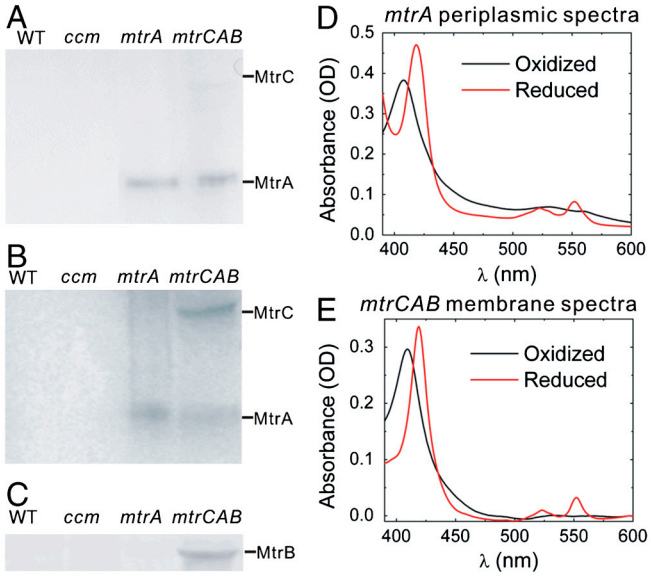

Fig. 2. Expression of full-length redox-active MtrA and MtrC in *E. coli*. Heme-stained SDS-PAGE gels of (*A*) periplasmic fractions and (*B*) membrane fractions of the WT, *ccm*, *mtrA*, and *mtrCAB* strains. (*C*) Anti-MtrB immunoblot of membrane fractions of the WT, *ccm*, *mtrA*, and *mtrCAB* strains. (*D*) Absorption spectra of the periplasmic fraction of the *mtrA* strain under oxidizing and reducing conditions. (*E*) Absorption spectra of the membrane fraction of the *mtrCAB* strain under oxidizing and reducing conditions.

552 nm. The periplasmic fractions of *mtrA and mtrCAB* strains and the membrane fraction of *mtrCAB* all exhibited signature absorption spectra typical of oxidized and reduced c-type cytochrome (Fig. 2 *D* and *E*). Additionally, using $A_{552\,\mathrm{nm}}$ of the periplasmic fractions and the extinction coefficient of purified MtrA ($\varepsilon_{552} = 28\ \mathrm{mM^{-1}\,cm^{-1}\,heme^{-1}}$) (33), we estimate that there are 4,000 and 2,100 redox active MtrA present per cell in the *mtrA* and *mtrCAB* strains, respectively. Assuming the same extinction coefficient for MtrC, we estimate there are 75 redox active MtrC per cell. Taken together, these data demonstrate that redox active, full-length MtrA and MtrC were heterologously expressed in *E. coli* with their native localization.

Expression of *S. oneidensis* MR-1 Cytochromes in *E. coli* Increases Soluble Fe(III) Citrate Reduction Rates. We next sought to determine whether heterologous expression of MtrA and MtrC in *E. coli* enabled in vivo reduction of soluble chelated iron species, which diffuse into the periplasm. To test iron reduction in live cultures, we added 10 mM Fe(III) citrate separately to sterile media or a fixed concentration ($OD_{600} = 0.5$) of heat-killed, WT, *ccm*, *mtrA*, and *mtrCAB* cells under anaerobic conditions and measured the Fe(II) concentration of the resulting cultures as a function of time using the ferrozine assay (43). For each time point, the Fe(II) concentration at that time was subtracted by the corresponding Fe(II) concentration in media-only sample, representing abiotic Fe(III) reduction, and normalized by the ratio of the original OD_{600} to the current OD_{600} to account for the relative number of cells at each time point.

As shown in Fig. 3, metabolically inactive heat-killed *E. coli* showed a small amount of Fe(III) reduction over the 10-d period that is most likely caused by nonmetabolic processes that have remained unidentified to date (44). Living strains reduce Fe(III) citrate at a rate above the metabolically inactive *E. coli* that is nearly identically for the first 2 d. After 2 d, the rate of Fe(III) reduction in the WT strain levels off ($10 \pm 2\ \mu\mathrm{M\,d^{-1}}$). The *ccm* strain reduces Fe(III) at a slightly faster rate ($33 \pm 3\ \mu\mathrm{M\,d^{-1}}$). Because increased expression of native *E. coli* c-type cytochromes slightly increases iron reduction (32), we tentatively assign this rate increase to *E. coli* c-type cytochromes resulting from the

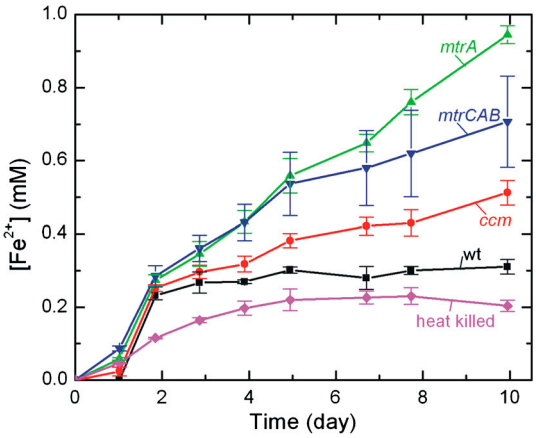

Fig. 3. Reduction of 10 mM Fe(III) citrate to Fe(II) as a function of time for the WT, *ccm*, *mtrA*, and *mtrCAB E. coli* strains. Error bars represent the standard deviation between triplicates from separate starting cultures.

overexpression of the *ccm* operon. In striking contrast, the average rates of reduction in the *mtrA* ($83 \pm 3\ \mu\mathrm{M\,d^{-1}}$) and *mtrCAB* ($59 \pm 11\ \mu\mathrm{M\,d^{-1}}$) strains are ~8 and ~6 times greater, respectively, than the rate of WT reduction. We attribute the dramatic changes in Fe(III) reduction rate in the *mtrA* and *mtrCAB* strains to the presence of the heterologous cytochromes c expressed in each strain. Surprisingly, the *mtrCAB* strain reduced Fe(III) at a lesser rate than the *mtrA* strain. We suggest that this could be due to decreased expression of MtrA in the *mtrCAB* strain and its preferential ability over MtrC to reduce Fe(III) citrate.

The Redox State of MtrA Is Kinetically Linked to Fe(III) Citrate Reduction in *E. coli*. The increase in Fe(III) citrate reduction in the *mtrA* strains relative to the *ccm* strain suggests that MtrA directly reduces Fe(III) citrate. To confirm this, we simultaneously measured Fe(II) concentration and monitored the α-band absorption at 552 nm in high-density anaerobic cell suspensions of the *mtrA* strain before and after adding 50 μM Fe(III) citrate. In order to clearly detect the α-band of MtrA over cell scatter and to observe Fe(II) formation over a shorter time scale, these experiments required unusually high cell densities and much lower concentrations of Fe(III) citrate; however, changes in the α-band absorption could be unambiguously detected even with an OD_{600} around 3.0 (Fig. 4*A*). Before the addition of Fe(III) citrate, the UV-Vis spectrum showed that MtrA is in a reduced state (black line). Upon Fe(III) addition, the α-band absorption immediately decreased (red line), indicating MtrA is rapidly oxidized. As time elapsed, the α-band absorption increased (dashed lines), indicating that MtrA is rereduced, presumably by cellular species.

Closer analysis can be undertaken by plotting $\Delta A_{552\,\mathrm{nm}}$ and Fe(II) concentration as a function of time relative to Fe(III) citrate addition (Fig. 4*B*). Immediately following Fe(III) citrate addition, the $A_{552\,\mathrm{nm}}$ decreases by ~0.15 OD and dwells in this oxidized state for 12 min. Over the same time period, ~30 μM is reduced to Fe(II). These observations provide a direct link between the time scales of MtrA oxidation and Fe(III) reduction in a heterologous host and strongly suggest that MtrA directly reduces Fe(III). They also suggest that movement of Fe(III) and Fe(II) in and out of the periplasm is extremely fast. Interestingly, after these fast initial events, the remaining Fe(III) is gradually converted to Fe(II) while MtrA is slowly rereduced to its initial redox state. The instantaneous rate of Fe(III) reduction decreasing as a function of time indicates that the reduction rate depends on the concentration of remaining Fe(III). This would be expected for any nonzeroth order chemical reaction. The slow rereduction of MtrA indicates that native *E. coli* proteins (e.g.,

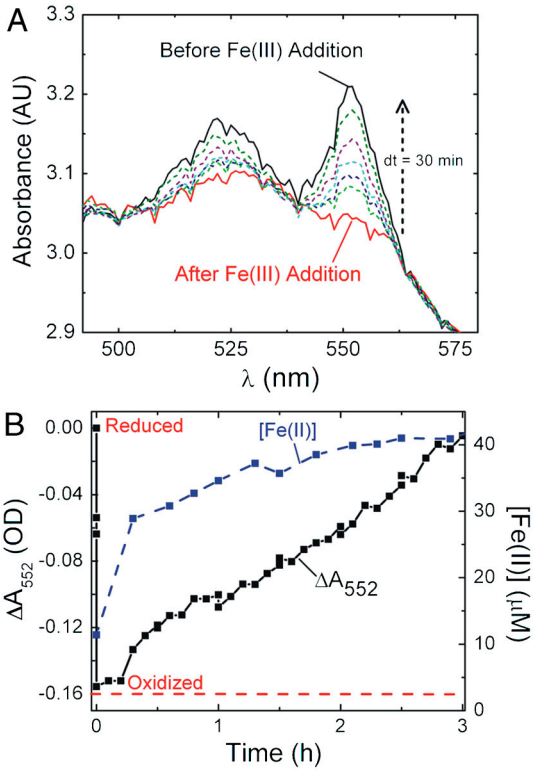

Fig. 4. Direct link of MtrA redox state to Fe(III) citrate reduction. (*A*) Absorption spectra showing the α-band of MtrA in high-density, anaerobic cell suspensions of the *mtrA* strain before and after the addition of Fe(III) citrate. MtrA begins reduced (black line, strong α-band absorption), but is oxidized upon the addition of 50 μM Fe(III) citrate (red line). Over time, the α-band absorbance recovers (colored dotted lines). (*B*) $\Delta A_{552\,nm}$ and Fe(II) concentration immediately before and after Fe(III) citrate addition as measured by the ferrozine assay.

NapC) are capable of reducing MtrA, but that this process is quite slow relative to the oxidation of MtrA by Fe(III).

NapC Is not the Only Electron Donor to MtrA in *E. coli*. Although the data in Fig. 4*B* show that MtrA is capable of being rereduced, it does not indicate which *E. coli* native protein(s) pass electrons from the quinol pool to MtrA in the periplasm. Previous work has suggested that NapC, a native *E. coli* inner membrane tetraheme cytochrome c, could functionally replace CymA, *S. oneidensis* MR-1's inner membrane tetraheme cytochrome c, because of the 52% sequence similarity (31). If NapC is the sole electron donor to MtrA, then we expect that an *E. coli* strain expressing *ccmA-H* and *mtrA* but lacking *napC* would reduce soluble Fe(III) at the same rate as the *ccm* strain. To explore this hypothesis, a *napC* knockout was made in BL21(DE3) using the λ-red gene disruption method (45). This strain, Δ*napC*, was cotransformed with *ccm* and/or *mtrA* to create the Δ*napC ccm* and Δ*napC mtrA* strains, which were analyzed for their ability to reduce soluble Fe (III) citrate. As shown in Fig. 5, the Δ*napC ccm* strain reduces Fe (III) more slowly than the *ccm* strain (21 ± 1 vs. 33 ± 3 μM d^{-1}, respectively), which is in accord with previous reports that suggested increased expression of NapC could enable soluble iron reduction in *E. coli* (31). Interestingly, the Δ*napC mtrA* strain reduces Fe(III) more slowly than the *mtrA* strain (51 ± 6 vs. 83 ± 3 μM d^{-1}, respectively). If NapC were the only protein transferring electrons from *E. coli* inner membrane to MtrA, it would be expected that the Δ*napC mtrA* strain reduction rate would be similar to that of the Δ*napC ccm* strain. However, destroying NapC expression does not completely diminish the

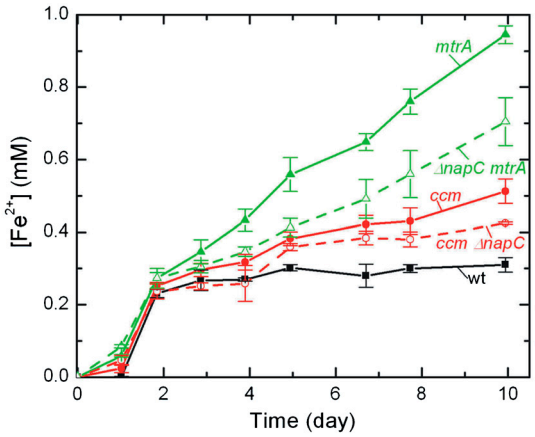

Fig. 5. NapC is not the sole electron donor to MtrA. Reduction of 10 mM Fe (III) citrate to Fe(II) by WT, ccm, Δ*napC ccm*, *mtrA*, and Δ*napC mtrA* strains.

reduction rate to that of the Δ*napC ccm* strain, suggesting that there are other electron donors to MtrA.

MtrCAB in *E. coli* Reduces Solid α-Fe_2O_3. Because our primary interest is in exploring a previously undescribed approach to electronically connect living cells and inorganic materials, we sought to determine whether the *mtrCAB* cluster is capable of reducing extracellular metal oxides. To test if heterologous expression of *mtrCAB* would reduce solid Fe_2O_3, we added α-Fe_2O_3 (Fig. 6*A*, $d \sim 5$ μm) to a final concentration of 2.5 mg mL^{-1} separately to sterile media or a fixed concentration ($OD_{600} = 1.0$) of WT, *ccm*, *mtrA*, and *mtrCAB* cells under anaerobic conditions, and measured the Fe(II) concentration and cfu of the resulting cultures as a function of time. The Fe(II) concentrations were normalized by cfu mL^{-1} at each time point. Figure 6*B* shows a representative time point ($t = 24$ d) of bulk α-Fe_2O_3 reduction for all strains. Very little solid Fe(III) is reduced by the WT, *ccm*, and *mtrA* strains; no solid α-Fe_2O_3 reduction is expected from the *E. coli* strains unless there is a complete electron transfer pathway that crosses both membranes because the *E. coli* genome does not encode for any proteins capable of transferring electrons from

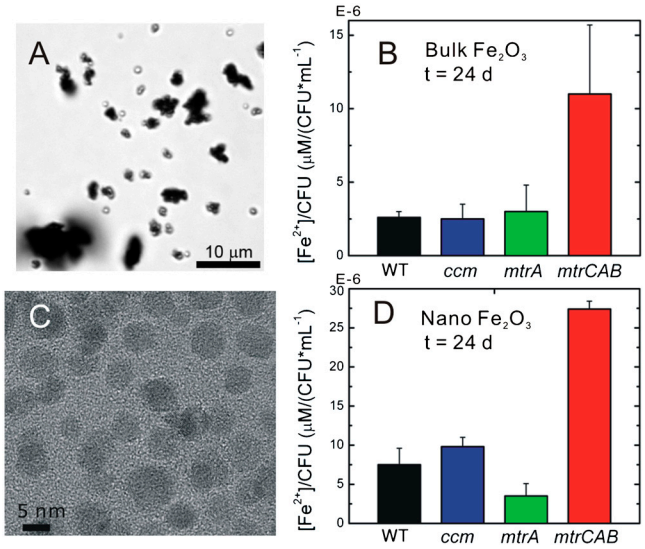

Fig. 6. MtrCAB reduces solid α-Fe_2O_3. (*A*) Brightfield optical image of bulk α-Fe_2O_3, $d \sim 5$ μm. (*B*) The concentration of bulk α-Fe_2O_3 reduced by WT, *cmm*, *mtrA*, *mtrCAB* strains normalized by colony forming units after 24 d. (*C*) Transmission electron microscopy of crystalline α-Fe_2O_3 nanoparticles, $d = 13$ nm. (*B*) The concentration of α-Fe_2O_3 nanoparticles reduced by WT, *ccm*, *mtrA*, *mtrCAB* strains normalized by colony forming units after 24 d.

the periplasm to the extracellular space. Interestingly, the *mtrCAB* strain reduces significant amounts of α-Fe_2O_3 per live cell ($11 \pm 5 \times 10^{-6}$ μM/cfu mL^{-1}) in comparison to the WT strain ($2.6 \pm 0.4 \times 10^{-6}$ μM/cfu mL^{-1}). Thus by expressing only three proteins from *S. oneidensis* MR-1, we are able to create a previously undescribed electron transfer pathway in *E. coli*, which transfers cytosolic electrons to the surface of extracellular α-Fe_2O_3. Additionally, these in vivo data provide further evidence to existing in vitro data that MtrA, MtrB, and MtrC are necessary and sufficient to reduce extracellular metal oxides.

Electron transfer theory predicts that in order for the *mtrCAB* strain to reduce α-Fe_2O_3, the MtrC-containing outer membrane must come into physical contact with the solid surface (46). This suggests that the rate of extracellular iron reduction by the *mtrCAB* strain would increase with increased α-Fe_2O_3 surface area. To test this prediction, we synthesized crystalline α-Fe_2O_3 nanoparticles (Fig. 6*C*, $d = 13$ nm), added these particles to a final concentration of 0.25 mg mL^{-1} to the WT, *ccm*, *mtrA*, and *mtrCAB* strains, and measured the formation of Fe(II) as described above. As in the bulk Fe_2O_3 experiments, WT, *ccm*, and *mtrA* strains show very little reduction of Fe_2O_3 in comparison to the *mtrCAB* strain ($27 \pm 1 \times 10^{-6}$ μM/cfu mL^{-1}). Moreover, the amount of Fe(III) reduced was ~2.5-fold greater for α-Fe_2O_3 nanoparticles than micron-sized α-Fe_2O_3 over the same time period despite the fact that Fe_2O_3 concentration was 10-fold lower.

Discussion

Engineering an efficient means of electronic communication between living and nonliving systems has the potential to create hybrid sensors and electronics capable of self-replication and -repair. Although existing technologies can transfer electrons from a cell to an electrode, no single approach has achieved what the next generation applications require: molecularly defined electron flow across a variety of cell types. Here we have demonstrated the feasibility of a wholly biological approach that meets this challenge and provides a previously undescribed blueprint for cellular-electronic connections. By the addition of previously undescribed genetic information, we have engineered electronic communication between living cells and inorganic materials. The genetic nature of this approach makes it applicable to many cell types and specifies the route for electron transfer. To transfer the system to a different prokaryote would simply require the choice of an appropriate promoter and origin of replication, use of a host-specific signal sequence to ensure proper localization, and modification of the *ccm* genes to achieve their expression under aerobic conditions.

Another unique advantage is that the cell directs the assembly of these bioelectronic connections such that they are self-repairing, requiring no experimenter assembly or intervention. Finally, based on the natural system's respiratory versatility, we anticipate that our engineered system should be able to reduce multiple types of inorganic electrodes.

Although this work achieves a molecularly defined electron conduit that may be introduced into other cell types, it is useful to compare the rate at which our engineered strains reduce Fe (III) to both WT *E. coli* and *S. oneidensis* MR-1 as a means of determining its relative efficiency. The *mtrCAB* strain reduces soluble and insoluble Fe(III) ~6-fold and ~4-fold faster, respectively, than WT *E. coli*; however, compared to *S. oneidensis* MR-1, the *mtrCAB* strain reduces soluble and insoluble Fe(III) ~30-fold and ~10-fold more slowly (47, 48). This rate difference suggests there is still room to optimize the efficiency and speed of the electron transfer pathway in our engineered strain.

In the case of soluble Fe(III) reduction, the transfer of electrons from native proteins of *E. coli* to MtrA is very likely the rate limiting step. The observation that no native *E. coli* cytochromes are detectable by TMBZ staining whereas MtrA is readily detectable (Fig. 2) indicates there is a relatively low ratio of electron donors to electron acceptors. The slow rereduction of MtrA in the high cell density experiments (Fig. 4) also supports this hypothesis. The rate of this initial electron transfer step may potentially be enhanced either by increasing the expression of native *E. coli* inner membrane cytochromes that donate electrons to MtrA (such as NapC) or by additionally expressing the native electron donor of MtrA, the *S. oneidensis* MR-1 inner membrane cytochrome CymA. These approaches could potentially translate into an increase in soluble Fe(III) reduction rate.

For solid Fe_2O_3 reduction, it is likely that the last step in the electron transport chain, reduction of Fe(III) by MtrC, is the rate limiting step. Because our data, as well as other studies (28, 49, 50), indicate that MtrC is the only significant donor of electrons to Fe_2O_3 (Fig. 6), the relatively low abundance of MtrC relative to MtrA (75 vs. 2,100 per cell, respectively) is a plausible explanation of why the *mtrCAB* strain does not reduce solid Fe(III) at the rates of *S. oneidensis* MR-1. Given the relative simplicity of our genetic device, future work will focus on optimizing expression of MtrC to improve overall electron transfer rates to extracellular metal oxides.

The increase in reduction rate for nanocrystalline α-Fe_2O_3 also suggests that materials engineering as well as synthetic biology will play a substantial role in optimizing electron transfer between engineered cells and inorganic materials. The *mtrCAB* strain generated 2.5-fold more Fe(II) from the α-Fe_2O_3 nanoparticles than bulk α-Fe_2O_3 over the same time period, even though the Fe_2O_3 concentration was 10-fold less. Although this is a significant rate enhancement, the surface area of the nanoparticles ($d = 13$ nm) is about 4 million times greater than the bulk α-Fe_2O_3 ($d \sim 5$ μm), indicating that the reduction rate does not scale linearly with the surface area. The nanocrystalline Fe_2O_3 is coated with citric acid to make the nanoparticles water-dispersible, and we speculate that this organic layer may modulate electron transfer from MtrC to the solid Fe_2O_3.

In summary, we have installed a unique electron transfer pathway in *E. coli* that allows intracellular electrons to be shuttled to the outer membrane where extracellular solid metal oxides can be reduced. These experiments demonstrate that *mtrCAB* is a genetic cassette that creates a molecularly defined pathway for electrons to move between living cells and inorganic materials. We envision that by installing this electronic pathway into organisms that evolve intracellular electrons in response to light, we could create extremely cheap, self-replicating photocatalysts that directly store energy in batteries. Additionally by combining our platform with organisms that modulate gene expression in response to small molecules, we could create living biosensors that provide electrical readouts. More broadly, our approach demonstrates that synthetic biology can be used to radically alter the materials properties of living cells much in the way that materials engineering can be used to alter physical properties of materials. Because this is an effective method to functionally interface cells with inorganic nanomaterials, we anticipate that this synthetic biology approach will find application in a host of nanobiotechnologies and bioelectronics.

Materials and Methods

Additional details can be found in *SI Text*.

Strains and Plasmids. The *mtrA* gene and *mtrCAB* cluster were amplified by PCR using *S. oneidensis* MR-1 genomic DNA as the template, and the PCR products were ligated into a modified pET30a+ vector (Novagen). The resulting plasmids were simultaneously transformed with a cytochrome c maturation plasmid, pEC86, into *E. coli* BL21(DE3) (Invitrogen). The Δ*napC* deletion strain was made using the λ-red strategy as described by Datsenko and Wanner (45).

Subcellular Fractionation. The periplasmic and membrane fractionation was performed as described by Londer et al. (51) and Nikaido (52), respectively.

Iron Reduction Assay Using Ferrozine. Cells from 50-mL cultures were pelleted, washed, and resuspended to an OD_{600} of 0.5 in anaerobic supplemented M9 minimal. All subsequent steps were performed in an anaerobic chamber (Coy Laboratory Products) with an environment of 2% H_2 balanced in N_2. Fe(III) citrate (Sigma) was added to a final concentration of 10 mM, and at the time of addition and subsequent time points, aliquots were removed to determine the optical density at 600 nm and Fe(II) concentration. The Fe(II) concentration was determined with the ferrozine assay, adapted from Stookey (43).

Cytochrome c Redox Assay in Intact Cells. Dense cell suspensions in anaerobic M9 minimal media supplemented with 0.4% lactate were transferred into sealable quartz cuvettes in an anaerobic chamber. The absorption spectrum of each culture was measured before iron addition, immediately after addition of 50 μM Fe(III)citrate, and at regular intervals afterward to observe changes in the redox state of the cytochromes. The concentration of Fe(II) was simultaneously monitored via the ferrozine assay.

Synthesis of α-Fe_2O_3(citrate)$_n$ Nanoparticles. α-Fe_2O_3(citrate) nanoparticles were synthesized using a two-step approach. Oleate passivated nanocrystals were prepared according to a modified, previously published literature procedure (53). The oleate shell was subsequently displaced with citric acid before aqueous transfer into buffer.

Reduction of Bulk and Nano Fe_2O_3. Cells from 50-mL cultures were pelleted, washed, and resuspended in anaerobic M9 minimal media to a final OD_{600} of 1.0. All subsequent steps were performed in an anaerobic chamber. For the bulk Fe_2O_3 assay, 50 mg of particulate Fe_2O_3 (Sigma) and 20 mL of anaerobic culture were added to a sterile bottle, yielding a final Fe_2O_3 concentration of 2.5 mg mL^{-1}. For nanoparticle cultures, the anaerobic nanoparticle solution (4 mg mL^{-1}) was added to a final concentration of 0.25 mg mL^{-1}.

ACKNOWLEDGMENTS. We thank Steven W. Singer (Lawrence Berkeley National Lab, Berkeley, CA) for providing the *ccm* plasmid pEC86 and Prof. Daad Saffarini (University of Wisconsin–Milwaukee, Milwaukee, WI) for a generous gift of the anti-MtrB antibody. This work, carried out at the Molecular Foundry, and H.M.J. were supported by the Office of Science, Office of Basic Energy Sciences, of the U.S. Department of Energy under Contract DE-AC02-05CH11231.

1. Patolsky F, et al. (2006) Detection, stimulation, and inhibition of neuronal signals with high-density nanowire transistor arrays. *Science* 313:1100–1104.
2. Ionescu-Zanetti C, et al. (2005) Mammalian electrophysiology on a microfluidic platform. *Proc Natl Acad Sci USA* 102:9112–9117.
3. Marsili E, et al. (2008) Shewanella secretes flavins that mediate extracellular electron transfer. *Proc Natl Acad Sci USA* 105:3968–3973.
4. Park DH, Zeikus JG (2000) Electricity generation in microbial fuel cells using neutral red as an electronophore. *Appl Environ Microbiol* 66:1292–1297.
5. Gunawardena A, Fernando S, To F (2008) Performance of a yeast-mediated biological fuel cell. *Int J Mol Sci* 9:1893–1907.
6. Rabinowitz JD, Vacchino JF, Beeson C, McConnell HM (1998) Potentiometric measurement of intracellular redox activity. *J Am Chem Soc* 120:2464–2473.
7. Kim HJ, et al. (2002) A mediator-less microbial fuel cell using a metal reducing bacterium, *Shewanella putrefaciens*. *Enzyme Microb Tech* 30:145–152.
8. Bond DR, Lovley DR (2003) Electricity production by *Geobacter sulfurreducens* attached to electrodes. *Appl Environ Microbiol* 69:1548–1555.
9. Rabaey K, Boon N, Siciliano SD, Verhaege M, Verstraete W (2004) Biofuel cells select for microbial consortia that self-mediate electron transfer. *Appl Environ Microbiol* 70:5373–5382.
10. Alferov S, et al. (2009) Electrical communication of cytochrome enriched *Escherichia coli* JM109 cells with graphite electrodes. *Electrochim Acta* 54:4979–4984.
11. Coman V, et al. (2009) Electrical wiring of live, metabolically enhanced *Bacillus subtilis* cells with flexible osmium-redox polymers. *J Am Chem Soc* 131:16171–16176.
12. Collier JH, Mrksich M (2006) Engineering a biospecific communication pathway between cells and electrodes. *Proc Natl Acad Sci USA* 103:2021–2025.
13. Daraselia N, et al. (2003) Reannotation of *Shewanella oneidensis* genome. *Omics* 7:171–175.
14. Vogel JP, et al. (2010) Genome sequencing and analysis of the model grass *Brachypodium distachyon*. *Nature* 463:763–768.
15. Benner SA, Sismour AM (2005) Synthetic biology. *Nat Rev Genet* 6:533–543.
16. Gardner TS, Cantor CR, Collins JJ (2000) Construction of a genetic toggle switch in *Escherichia coli*. *Nature* 403:339–342.
17. Andrianantoandro E, Basu S, Karig DK, Weiss R (2006) Synthetic biology: New engineering rules for an emerging discipline. *Mol Syst Biol* 2:0028.
18. Serrano L (2007) Synthetic biology: Promises and challenges. *Mol Syst Biol* 3:158.
19. Lu TK, Khalil AS, Collins JJ (2009) Next-generation synthetic gene networks. *Nat Biotechnol* 27:1139–1150.
20. Khalil AS, Collins JJ (2010) Synthetic biology: Applications come of age. *Nat Rev Genet* 11:367–379.
21. Ro D, et al. (2006) Production of the antimalarial drug precursor artemisinic acid in engineered yeast. *Nature* 440:940–943.
22. Gibson DG, et al. (2010) Creation of a bacterial cell controlled by a chemically synthesized genome. *Science* 329:52–56.
23. Myers CR, Nealson KH (1988) Bacterial manganese reduction and growth with manganese oxide as the sole electron acceptor. *Science* 240:1319–1321.
24. Shi L, Squier TC, Zachara JM, Fredrickson JK (2007) Respiration of metal (hydr)oxides by Shewanella and Geobacter: A key role for multihaem c-type cytochromes. *Mol Microbiol* 65:12–20.
25. Gralnick JA, Newman DK (2007) Extracellular respiration. *Mol Microbiol* 65:1–11.
26. Shi L, et al. (2009) The roles of outer membrane cytochromes of *Shewanella* and *Geobacterin* extracellular electron transfer. *Environ Microbiol Rep* 1:220–227.
27. Myers C, Myers J (2004) The outer membrane cytochromes of *Shewanella oneidensis* MR-1 are lipoproteins. *Lett App Microbiol* 39:466–470.
28. Hartshorne R, et al. (2007) Characterization of *Shewanella oneidensis* MtrC: A cell-surface decaheme cytochrome involved in respiratory electron transport to extracellular electron acceptors. *J Biol Inorg Chem* 12:1083–1094.
29. Ross DE, et al. (2007) Characterization of protein-protein interactions involved in iron reduction by *Shewanella oneidensis* MR-1. *Appl Environ Microbiol* 73:5797–5808.
30. Reardon CL, et al. (2010) Role of outer-membrane cytochromes MtrC and OmcA in the biomineralization of ferrihydrite by *Shewanella oneidensis* MR-1. *Geobiology* 8:56–68.
31. Gescher JS, Cordova CD, Spormann AM (2008) Dissimilatory iron reduction in *Escherichia coli*: Identification of CymA of *Shewanella oneidensis* and NapC of *E. coli* as ferric reductases. *Mol Microbiol* 68:706–719.
32. Schuetz B, Schicklberger M, Kuermann J, Spormann AM, Gescher J (2009) Periplasmic electron transfer via the c-type cytochromes MtrA and FccA of *Shewanella oneidensis* MR-1. *Appl Environ Microbiol* 75:7789–7796.
33. Pitts KE, et al. (2003) Characterization of the *Shewanella oneidensis* MR-1 decaheme cytochrome MtrA. *J Biol Chem* 278:27758–27765.
34. Donald JW, Hicks MG, Richardson DJ, Palmer T (2008) The c-type cytochrome OmcA localizes to the outer membrane upon heterologous expression in *Escherichia coli*. *J Bacteriol* 190:5127–5131.
35. Myers CR, Myers JM (2002) MtrB is required for proper incorporation of the cytochromes OmcA and OmcB into the outer membrane of *Shewanella putrefaciens* MR-1. *Appl Environ Microbiol* 68:5585–5594.
36. Beliaev AS, Saffarini DA (1998) *Shewanella putrefaciens* mtrB encodes an outer membrane protein required for Fe(III) and Mn(IV) reduction. *J Bacteriol* 180:6292–6297.
37. Dubendorf JW, Studier FW (1991) Controlling basal expression in an inducible T7 expression system by blocking the target T7 promoter with lac repressor. *J Mol Biol* 219:45–59.
38. Studier FW, Rosenberg AH, Dunn JJ, Dubendorff JW (1990) Use of T7 RNA polymerase to direct expression of cloned genes. *Method Enzymol* 185:60–89.
39. Thony-Meyer L, Fischer F, Kunzler P, Ritz D, Hennecke H (1995) *Escherichia coli* genes required for cytochrome c maturation. *J Bacteriol* 177:4321–4326.
40. Arslan E, Schulz H, Zufferey R, Künzler P, Thöny-Meyer L (1998) Overproduction of the *Bradyrhizobium japonicum* c-type cytochrome subunits of the *cbb*3 oxidase in *Escherichia coli*. *Biochem Biophys Res Comm* 251:744–747.
41. Thomas PE, Ryan D, Levin W (1976) An improved staining procedure for the detection of the peroxidase activity of cytochrome P-450 on sodium dodecyl sulfate polyacrylamide gels. *Anal Biochem* 75:168–176.
42. Myers CR, Myers JM (1992) Localization of cytochromes to the outer membrane of anaerobically grown *Shewanella putrefaciens* MR-1. *J Bacteriol* 174:3429–3438.
43. Stookey LL (1970) Ferrozine—A new spectrophotometric reagent for iron. *Anal Chem* 42:779–781.
44. Williams HD, Poole RK (1987) Reduction of iron(III) by *Escherichia coli* K12: Lack of involvement of the respiratory chains. *Curr Microbiol* 15:319–324.
45. Datsenko KA, Wanner BL (2000) One-step inactivation of chromosomal genes in *Escherichia coli* K-12 using PCR products. *Proc Natl Acad Sci USA* 97:6640–6645.
46. Wigginton NS, Rosso KM, Stack AG, Hochella J (2009) Long-range electron transfer across cytochrome-hematite (α-Fe2O3) interfaces. *J Phys Chem C* 113:2096–2103.
47. Jones ME, Fennessey CM, DiChristina TJ, Taillefert M (2010) *Shewanella oneidensis* MR-1 mutants selected for their inability to produce soluble organic-Fe(III) complexes are unable to respire Fe(III) as anaerobic electron acceptor. *Environ Microbiol* 12:938–950.
48. Bose S, et al. (2009) Bioreduction of hematite nanoparticles by the dissimilatory iron reducing bacterium *Shewanella oneidensis* MR-1. *Geochim Cosmochim Acta* 73:962–976.
49. Ross DE, Brantley SL, Tien M (2009) Kinetic characterization of OmcA and MtrC, terminal reductases involved in respiratory electron transfer for dissimilatory iron reduction in *Shewanella oneidensis* MR-1. *Appl Environ Microbiol* 75:5218–5226.
50. Wang Z, et al. (2008) Kinetics of reduction of Fe(III) complexes by outer membrane cytochromes MtrC and OmcA of *Shewanella oneidensis* MR-1. *Appl Environ Microbiol* 74:6746–6755.
51. Londer YY, Giuliani SE, Peppler T, Collart FR (2008) Addressing *Shewanella oneidensis* "cytochromome": The first step towards high-throughput expression of cytochromes c. *Protein Expres Purif* 62:128–137.
52. Nikaido H (1994) *Isolation of Outer Membranes in Bacterial Pathogenesis Part A: Identification and Regulation of Virulence Factors* (Academic, New York), pp 225–234.
53. Wang S, Min Y, Yu S (2007) Synthesis and magnetic properties of uniform hematite nanocubes. *J Phys Chem C* 111:3551–3554.

Supporting Information

Jensen et al. 10.1073/pnas.1009645107

SI Materials and Methods.

Strains and Plasmids. Primers containing EcoRI and XbaI restriction sites (Table S1, primers 1 and 2 for *mtrA*; primers 3 and 4 for *mtrCAB*), and Platinum Pfx Polymerase (Invitrogen) were used to amplify the respective sequences. After digestion with EcoRI and XbaI, these DNA fragments were ligated into the modified pET30a+ vector using T4 DNA Ligase (Roche). The modified pET30a+ vector had an NdeI site (CATATG) directly upstream of the EcoRI site used for insertion. The ATG in the NdeI site was used as the start codon, and the forward primers for PCR were designed to clone from the second codon of *mtrA and mtrC* in the Shewanella genome. This design adds the two codons from the EcoRI site coding Glu-Phe; however, the extra amino acids will be cleaved by the Sec system in the process signal sequence cleavage of MtrA and MtrC in plasmids *mtrA and mtrCAB*. respectively. The *ccm* plasmid, pEC86, encodes the genes *ccmA-H* under a tet promoter and carries a chloramphenicol resistance marker.

Construction of *napC* Deletion Strain. The plasmids used in the gene disruption process, pKD46, pKD3, pKD4, and pCP20, were obtained from the Coli Genetic Stock Center at Yale University. Primers 5 and 6 (Table S1) contain regions homologous to the region directly upstream and downstream, respectively. These primers were used to amplify a cassette containing kanamaycin resistance flanked by FLP recombinase recognition target sites off of pKD4 using Platinum Pfx Polymerase (Invitrogen). This PCR product was electroporated with BL21(DE3) expressing pKD46, induced with 10 mM L-arabinose, to replace *napC* in the *E. coli* BL21(DE3) genome. Cells were grown with antibiotic selection on kanamycin LB plates grown at 37 °C. Colony PCR using primers 7 and 8 (Table S1) was performed to verify the replacement in the genome. Kanamycin resistance was removed by electroporating the new strain with pCP20, which removes the sequence between the FRT sites. After pCP20 inactivation, colony PCR was performed using primers 7 and 8 to verify removal of the kanamycin resistance gene. The resulting strain is BL21 (DE3)Δ*napC*.

Cell Growth. All strains, unless otherwise specified, were grown in 2xYT media at 30 °C with 50 μg mL^{-1} kanamycin; strains containing the *ccm* plasmid were grown with an additional 30 μg mL^{-1} chloramphenicol. Glycerol stocks were used to inoculate 5 mL media, and cultures were grown overnight at 37 °C with 250-rpm shaking. Then 50 μL of overnight cultures were back-diluted into 5 mL media and grown with 250-rpm shaking for 12 h. For Fe(III) reduction assays, 50 mL of fresh 2xYTwas inoculated with 250 μL of the previous culture and then grown 16 h with 200-rpm shaking. For periplasmic and membrane fractionations, 5 mL of overnight culture were used to inoculate 1 L media and were grown for 16 h.

Periplasmic Fractionation. The cells from a 1-L culture were pelleted by centrifugation for 15 min at 4,000 × *g* and 4 °C. The resulting cell pellet was slowly resuspended to homogeneity in 30 mL of ice-cold *N*-[tris(hydroxymethyl)methyl]-2-aminoethanesulfonic acid, pH 8.0, by pressing the cells with a rubber policeman on the side of the flask. Chicken egg white lysozyme (Sigma) was added to the resuspended pellet to a final concentration 0.5 mg mL^{-1} and incubated at room temperature for 15 min. After addition of 30 mL of ice-cold water, the suspension was shaken horizontally on ice for 15 min at 100 rpm and then centrifuged at 12,000 × *g* for 20 min at 4 °C. The supernatant was collected as the periplasmic fraction while the outer membrane and intact cytoplasm was in the pellet. The periplasmic fraction was analyzed by SDS-PAGE heme-stained gels and by UV-Vis for redox spectral properties.

Membrane Fractionation. The cells from a 1-L culture were pelleted by centrifugation for 15 min at 4,000 × *g* and 4 °C and then washed in 1 L 10 mM Hepes, pH 7.4. The washed pellet was then resuspended in 120 mL ice-cold 10 mM Hepes, pH 7.4. Chicken egg white lysozyme was added to the cell suspension to a final concentration of 20 μg mL^{-1} and incubated at room temperature for 30 min. The protease inhibitor PMSF (Thermo Scientific) was added to a final concentration of 1 mM. The cells were disrupted via ultrasonication (power level 5, 9 min total duty in cycles of 30 s on, 30 s off, Misonix 3000, Misonix Inc.) in an ice bath. Unbroken cells were removed by centrifugation at 1,000 × *g* for 15 min, and the resulting supernatant was removed and centrifuged at 100,000 × *g* for 2 h at 4 °C to yield a pellet corresponding to the crude cell envelope, containing both the outer and inner membrane. This membrane fraction was solubilized in a solution of 5% (wt/vol) Triton X-100, 50 mM Hepes pH 7.4, 200 mM NaCl before analysis by SDS-PAGE, Western blotting, and UV-Vis spectroscopy. The supernatant of this spin was saved for analysis by SDS-PAGE.

TMBZ Peroxidase Stain of SDS-PAGE. The 3,3′,5,5′-tetramethylbenzidene (TMBZ) peroxidase stain method was adapted from Thomas (1) to identify cytochromes c. Protein samples were suspended in lithium dodecyl sulfate without β-mercaptoethanol. The samples were run in 12.5% Tris HCl polyacrylamide gel (BioRad) at 16 °C at 200 V for 60 min. TMBZ was dissolved in methanol to 6.3 mM and mixed 3 : 7 TMBZ solution:0.25 M Sodium acetate, pH 5. The gel was immersed in this mixture in the dark with occasional mixing for 2 h. Hydrogen peroxide was added to a final concentration of 30 mM, and bands were visualized 30 min after peroxide addition.

MtrB Western. Denatured membrane protein samples were electrophoresed in 12.5% polyacrylamide gel and transferred to nitrocellulose membranes. The primary antibody for MtrB (Rabbit Anti-MtrB) was kindly provided by Prof. Daad Saffarini (University of Wisconsin–Madison) and used at 1 : 10,000 dilution. The Immun-Star Goat Anti-Rabbit-HRP Conjugate kit was used as the secondary antibody at 1 : 60,000 dilution. The Western and visualization of bands was done as per the Immun-Star WesternC Chemiluminescent Kit (BioRad).

Visible Spectra of Cytochrome Samples. Samples from the periplasmic fraction and membrane fractionation were diluted such that the absorbance was within the linear range. Visible spectra of air-exposed samples were considered as fully oxidized protein samples. The protein was chemically reduced by adding sodium dithionite crystals (Sigma), and the spectrum was taken again. Membrane fractions were baseline subtracted to consider the scattering of light caused by Triton X-100 micelles.

Iron Reduction Assay Using Ferrozine. Cells from 50-mL cultures were pelleted, washed, and resuspended to an OD_{600} of 0.5 in anaerobic M9 minimal media (12.8 g L^{-1} Na_2HPO_4-$7H_2O$, 3.0 g L^{-1} KH_2PO_4, 0.50 g L^{-1} NaCl, 1.0 g L^{-1} NH_4Cl) (Difco) supplemented with 0.4% lactate (Alfa Aesar), 1 mM thiamine

HCl (Sigma), 0.2% casamino acids (Merck), 2.0 mM $MgSO_4$ (Aldrich), and 0.1 mM $CaCl_2$ (Aldrich). One aliquot of each culture was centrifuged at $4{,}000 \times g$ for 5 min at room temperature in the anaerobic chamber to pellet the cells, and the supernatant was acid extracted in 0.5 M HCl for 1 h. The total iron concentration was determined by a separate acid extraction with 10% hydroxylamine hydrochloride (Aldrich) in 0.5 M HCl for 1 h. An aliquot of each acid extracted sample was then added to the dye, ferrozine (Acros Organics) buffered in 100 mM Hepes, pH 8.0, which absorbs at 563 nm ($\varepsilon_{563\,\mathrm{nm}} = 27.9\ \mathrm{mM}^{-1}\ \mathrm{cm}^{-1}$) when bound to Fe (II). The absorbance of all samples was recorded at 563 nm with a UV-Vis spectrophotometer (Perkin–Elmer Lambda 35) and was used to determine the change of Fe(II) concentration over time as well as monitor total iron concentration available in the media. The concentration of Fe(II) in each culture was subtracted by any abiotic iron reduction observed in media controls at each time point and was normalized to the relative number of cells by multiplying by the factor $\frac{0.5}{\mathrm{OD600}_i}$. Error bars represent standard deviation by triplicate cultures.

Cytochrome c Redox Assay in Intact Cells. After apparent recovery of the redox state of the cytochrome, an additional 25 μM of Fe(III) citrate was added. The spectrum was monitored again with similar results. All spectra were normalized to the average absorbance at 561 nm, an approximate isobestic point. $\Delta A_{552\,\mathrm{nm}}$ was calculated by subtracting the initial $A_{552\,\mathrm{nm}}$ from all time points.

Synthesis of Fe_2O_3 Nanoparticles. Iron(III) chloride hexahydrate (544 mg, 2.01 mmol), sodium oleate (1.826 g, 6.00 mmol), oleic acid (1.0 mL, 3.14 mmol), absolute ethanol (5.0 mL), and H_2O (8.0 mL) were combined in a 20-mL microwave reaction vial and stirred for 1 h at 25 °C, giving an opaque, dark reddish-brown organic top layer and a clear, pale yellow aqueous bottom layer in the microwave vial. The reaction vessel was transferred to a microwave synthesizer (Biotage Initiator 8) and heated at 80 °C for 8 h, then at 180 °C for 15 min. The contents of the vessel were transferred to a 50-mL conical tube and centrifuged at $4{,}400 \times g$ for 30 min, affording a dark reddish-brown pellet of nanocrystals. The liquid portion was decanted off and the pellet washed sequentially with H_2O (5.0 mL) and absolute ethanol (5.0 mL). The pellet was resuspended in hexanes (50 mL), and the tube centrifuged at $4{,}400 \times g$ for 5 min., giving a clear, dark reddish-brown hexane solution containing smaller, soluble Fe_2O_3 nanoparticles, and a reddish-brown pellet containing larger, insoluble Fe_2O_3 nanoparticles and Fe_2O_3 nanoparticle aggregates. The hexanes solution was filtered through an Acrodisc Syringe Filter (0.22 μm, Pall Corporation), giving a clear, dark reddish-brown solution containing oleic acid-coated Fe_2O_3 nanoparticles. Dynamic light scattering (DLS) measurements (Malvern Instruments) performed in hexanes at 20 °C showed that the particles were narrowly distributed, with a mean diameter of 13 nm.

Fe_2O_3 nanoparticles were heated with citric acid (480 mg) in anhydrous DMSO (2.5 mL) at 100 °C for 24 h with stirring. The resulting solution was added slowly to 100 mL of 100 mM sodium tetraborate buffer, pH 10.0, with periodic adjustment of pH to 10 with NaOH (1.0 M), giving a clear, reddish-brown aqueous solution. The nanoparticles were concentrated by spin dialysis (Amicon Ultra-15 10 K MWCO, Millipore Corporation), and dialyzed with 5×15 mL of 10 mM sodium tetraborate buffer, pH 8.3. DLS measurements (Malvern Instruments) performed in buffer at 20 °C showed that the citrate-coated Fe_2O_3 particles were narrowly distributed, with a mean diameter of 13 nm.

Reduction of Bulk and Nano Fe_2O_3. At each time point, the colony forming units and Fe(II) concentration for each culture was measured. To determine colony forming units, dilutions of each culture were plated on LB plates supplemented with Kanamycin (to test for the presence of the *mtrA* or *mtrCAB* plasmids). Plates were grown at 30 °C for 24 h. The concentration of Fe(II) was determined by the ferrozine assay and was normalized for each culture by cfu. Error bars represent standard deviation by triplicate cultures.

1. Bose S, et al. (2009) Bioreduction of hematite nanoparticles by the dissimilatory iron reducing bacterium *Shewanella oneidensis* MR-1. *Geochim Cosmochim Acta* 73:962–976.

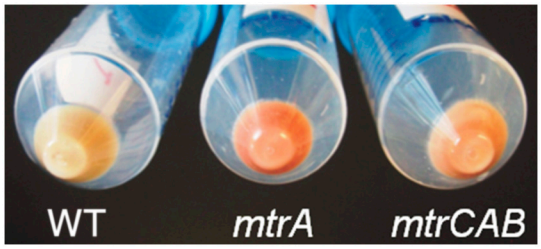

Fig. S1. Cell pellets of uninduced WT, *mtrA*, and *mtrCAB* strains. The red color is caused by the hemes. Interestingly, addition of as little as 10 μM IPTG to *mtrA* and *mtrCAB* cultures resulted in a less intense red color of the cell pellets and less intense MtrA and MtrC bands in the TMBZ stained whole cell extracts as compared to cultures containing no IPTG. Thus, basal expression of the *mtrA* and *mtrCAB* plasmids yields a higher concentration of correctly folded cytochrome c than induced expression.

Table S1. Primers

Primer no.	Sequence (5′–3′)
1	GGCCGAATTCAAGAACTGCCTAAAAATGAA
2	AACCTCTAGATTAGCGCTGTAATAGCTTGCCA
3	CCGCGAATTCATGAACGCACAAAAATCAAAAATCGC
4	CCGGTCTAGATTAGAGTTTGTAACTCATGCTC
5	CGCTCACAAAGTAACTCTCTGGCTTCAAGCATACCCACGCAATAACCCTG GTGTAGGCTGGAGCTGCTTC
6	TGGGGAATACCTTTACCCCATCAAAAGGTTACGGGAAATAAGAGGTTATT ATGGGAATTAGCCATGGTCC
7	CGCTCACAAAGTAACTCTCTGGCTT
8	TGGGGAATACCTTTACCCCATCAAA

Table S2. Plasmids

Plasmid	Promotor	Protein coding regions(s)	Antibiotic resistance	Source
pSB1ET2 (pET)	T7 lac	n/a	Kan	(This paper)
I5023	T7 lac	*mtrA*	Kan	(This paper)
I5024	T7 lac	*mtrCAB*	Kan	(This paper)
pEC86	Tet	*ccmA-H*	Chl	Steve Singer (Lawrence Berkeley National Lab, Berkeley, CA)
pKD46	P_{araB}	λ-red recombinase	Amp	Coli genetic stock
pKD3	NA	NA	Amp, Chl	Coli genetic stock
pKD4	NA	NA	Amp, Kan	Coli genetic stock
pCP20	NA	FLP	Amp	Coli genetic stock

NA, not applicable.

Table S3. Strains

Strain	Cell line	Plasmids	Gene(s)
wt	BL21(DE3)	pSB1ET2 empty vector	None
ccm	BL21(DE3)	pSB1ET2_empty + pEC86	*ccmA-H*
mtrA	BL21(DE3)	pSB1ET2_MtrA + pEC86	*mtrA, ccmA-H*
mtrCAB	BL21(DE3)	pSB1ET2_MtrCAB + pEC86	*mtrCAB, ccmA-H*
Δ*napC*	BL21(DE3)Δ*napC*	pSB1ET2 empty vector	None
Δ*napC ccm*	BL21(DE3)Δ*napC*	pSB1ET2_empty + pEC86	*ccmA-H*
Δ*napC mtrA*	BL21(DE3)Δ*napC*	pSB1ET2_MtrA + pEC86	*mtrA, ccmA-H*
Δ*napC mtrCAB*	BL21(DE3)Δ*napC*	pSB1ET2_MtrCAB + pEC86	*mtrCAB, ccmA-H*